

# Task-Oriented Edge-Assisted Cooperative Data Compression, Communications and Computing for UGV-Enhanced Warehouse Logistics

Jiaming Yang<sup>1</sup>, Zhen Meng<sup>1</sup>, Xiangmin Xu<sup>1</sup>, Kan Chen<sup>1</sup>, Emma Liying Li<sup>1</sup>, Philip G. Zhao<sup>2</sup>

<sup>1</sup>*School of Computer Science, University of Glasgow, UK*

<sup>2</sup>*Department of Computer Science, University of Manchester, UK*

{j.yang.9, x.xu.1, k.chen.1}@research.gla.ac.uk,

{zhen.meng, liying.li}@glasgow.ac.uk, philip.zhao@manchester.ac.uk

**Abstract**—This paper explores the growing need for task-oriented communications in warehouse logistics, where traditional communication Key Performance Indicators (KPIs)—such as latency, reliability, and throughput—often do not fully meet task requirements. As the complexity of data flow management in large-scale device networks increases, there is also a pressing need for innovative cross-system designs that balance data compression, communication, and computation. To address these challenges, we propose a task-oriented, edge-assisted framework for cooperative data compression, communication, and computing in Unmanned Ground Vehicle (UGV)-enhanced warehouse logistics. In this framework, two UGVs collaborate to transport cargo, with control functions—navigation for the front UGV and following/conveyance for the rear UGV—offloaded to the edge server to accommodate their limited on-board computing resources. We develop a Deep Reinforcement Learning (DRL)-based two-stage point cloud data compression algorithm that dynamically and collaboratively adjusts compression ratios according to task requirements, significantly reducing communication overhead. System-level simulations of our UGV logistics prototype demonstrate the framework’s effectiveness and its potential for swift real-world implementation.

**Index Terms**—Task-oriented, cooperative, warehousing, edge computing

## I. INTRODUCTION

Warehousing plays an essential role within the supply chain by serving as a crucial hub for systematic storage, meticulous management, and streamlined distribution of cargos. It serves as a strategic node where inventory is carefully organized, monitored, and prepared for timely delivery to meet consumer demands and operational requirements within various industries [1]. Modern warehouses are progressively incorporating advanced technologies such as Artificial Intelligence (AI) and robotics to facilitate intelligent automation of tasks [2]. However, the deployment of these technologies necessitates extensive data transmission (e.g. radar, camera, and GPS), real-time responsiveness (e.g. decision making for autonomous navigation), and substantial machine-type communications (e.g. multi-Unmanned Ground Vehicle (UGV) coordination). Despite these requirements aligning with the three typical 5G services defined by 3GPP—enhanced Mobile Broadband (eMBB), massive Machine-Type Communications (mMTC),

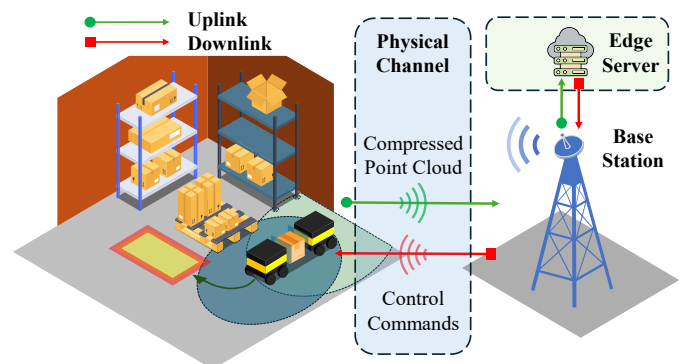


Fig. 1. Edge computing enabled autonomous driving.

and Ultra-Reliable Low-Latency Communications (URLLC)—they still do not fully meet the stringent demands of warehouse applications [3], [4]. This is particularly true as more complex tasks emerge in the foreseeable future [2]. Due to the limited communication capabilities and computational load of UGV in warehouse logistics scenarios, edge computing has emerged as a potential solution [5], [6]. By offloading computational tasks to edge servers, UGVs can achieve more powerful intelligence, reduced communication, and computational resource overhead, and significantly faster response and decision-making capabilities [7].

From a machine’s perspective, achieving a perfectly accurate reconstruction is deemed sufficient but unnecessary for task completion, as it often contains redundant information. The ultimate objective of transmission is to facilitate the completion of subsequent tasks. Based on that, task-oriented communication is gradually gaining attention [8]. It follows Shannon’s second and third ideas, moving away from the bit-centric communication principles towards a communication design approach that focuses on meeting semantic and task requirements [9]. This communication design approach is also gradually being applied in wide-ranging applications, including robotics [10], autonomous driving [11], and metaverse [12] scenarios.

However, task-oriented communications still face bottlenecks in UGV-enhanced warehouse logistic applications, including: 1) Gap between traditional Communication Key Performance Indicatorss (KPIs) and Task-oriented KPIs: The more detailed and intricate scenarios within warehouse applications involve complex interactions with their surroundings. As a result, connecting traditional communication KPIs (e.g. latency, throughput, and reliability) to the success of tasks becomes difficult. This difficulty arises because these complex interactions cannot be easily represented or measured using straightforward loss functions or performance metrics. 2) Seamless Data Sharing and Interpretation: Different submodules in warehouse logistics systems must seamlessly share and interpret data to perform cooperative tasks effectively. Therefore, managing these information pipelines requires cross-system designs that balance sampling, communication, and computation demands. This balance is crucial given the vast amounts of data generated by numerous devices and the need for real-time processing. 3) Scalability: As the number of UGVs increases, the efficient deployment of the AI algorithm becomes challenging. Therefore, how to handle complex information flows in large-scale UGV deployments in warehouses presents significant challenges.

To address these challenges, we propose a task-oriented edge-assisted cooperative data compression, communications, and computing framework for UGV-enhanced warehouse logistics. Specifically, we take typical warehouse logistics collaboration tasks, where two UGVs convey cargo boxes cooperatively to target positions, as example applications as the showcase [13]. Constrained by the on-board computing capacities of UGVs, we offload the two controllers of the UGVs; the front UGV for navigation and rear UGV for collaborated conveyance. To save communication overhead, we design a Deep Reinforcement Learning (DRL)-based two-stage point cloud data compression algorithm deployed on the edge server, where the compression ratios of the two UGVs are dynamically and collaboratively determined based on the task requirements. The major contributions of this work are summarized as follows:

- We propose a task-oriented edge-assisted framework for UGV-enhanced warehouse logistics, where the data compression, communications, and computing of front and rear UGVs are jointly considered for accomplishing collaborative cargo box conveyance and parking tasks. The functions of two controllers of two UGVs are offloaded to the edge server, and the compression rate of two UGVs are jointly and dynamically determined based on the channel conditions and task requirements.
- We proposed a two-stage DRL-based point cloud data compression algorithm to save the communication overhead, simultaneously exploiting the effectiveness of neural networks and the stability of model-based. Specifically, the data is first initially compressed by a data-based neural network compressor, then undergoes model-based compression and the compression length is dynamically

decided by a DRL-based agent.

- We developed a prototype and verified the robustness of the proposed algorithm in a warehouse environment alongside various baselines, where the Nvidia Isaac Sim platform is used. The experimental results demonstrate that our proposal significantly reduces communication overhead under different channel conditions which can be quickly deployed in the real world.

## II. RELATED WORK

Significant contributions have been made in the existing literature to improve the intelligence of different UGVs and reduce communication overhead. By processing data closer and offloading tasks to where it is generated, edge computing reduces latency and the amount of data transmitted to central servers, conserving bandwidth and improving response times [14]–[17]. In [15], the authors present cloud control of UGVs in future factories. By optimizing the coding rate threshold through control parameter adjustments, the study shows that communication-control co-design reduces coding rate requirements and wireless resource consumption, improving system stability and increasing the number of admissible UGVs. In [14], the authors address disaster scenarios by proposing Unmanned Aerial Vehicle (UAV)-assisted Mobile Edge Computing (MEC) as an alternative to damaged terrestrial infrastructure. They introduce a hierarchical architecture and an online optimization approach (OJTRTA) using game theory and convex optimization to improve Quality of Experience (QoE) and manage UAV resources. In [16], the authors address computation offloading in MEC systems with task dependencies by proposing a scheme that uses task migration and merging to minimize Deadline Violation Ratio (DVR). They introduce a multi-priority task sequencing algorithm and a Deep Deterministic Policy Gradient (DDPG)-based learning approach, achieving a 60.34% to 70.3% reduction in DVR compared to existing methods.

On the other hand, task-oriented communications have been applied in widespread applications scenarios including text [18], image [19], point cloud data transmission [20], and control [21] tasks. In [21], the authors propose a task-oriented semantics-aware (TOSA) communication framework for UAV control and command (C&C) transmissions to meet stringent Quality of Service (QoS) requirements. They define information value based on similarity and Age of Information (AoI) and use a DRL algorithm to maximize TOSA information. The work in [22] addresses optimizing communication for 5G and beyond in robotic swarms and industrial remote control systems. It proposes a dual approach using DRL and Vector Quantized Variational Autoencoders (VQ-VAE) to dynamically adjust data transmission for better accuracy and compression on the CartPole problem [11]. The authors in [23] further extend the task-oriented communications framework to the edge server, where the feature extraction, source coding, and channel coding are jointly designed and guided by information bottleneck (IB) theory. The results show that it can reduce communication overhead through a sparsity-

inducing distribution and adapt to dynamic channel conditions with variable-length encoding. In addition, there has been a lot of existing work focusing on task-oriented communication in multi-user situations and semantic communication in applications [24]–[28]. In [25], the author proposes a task-oriented communication-based framework for Multi-Agent systems, aiming to support efficient cooperation among agents. However, intrinsic connections between UGVs in warehouse logistics, especially in the context of relationships with collaborative tasks and conditions of resource competition, remain an open issue.

### III. SYSTEM MODEL

#### A. Overview

As shown in Fig. 1, two UGVs convey a cargo box collaboratively to park in a certain place. The function of the front UGV is to navigate to the desired parking place, and the role of the rear UGV is to follow and cooperate with the front UGV in conveying the cargo box. They both fulfill their tasks based on the captured 3-D point-cloud data from the onboard LiDAR. Constrained by their onboard computing capacities, we offload the two controllers of two UGVs to the edge server. That is, the captured 3-D point cloud data is first transmitted by the two UGVs via the uplink wireless channel. After receiving and processing by the edge server, the control commands of two UGVs are generated and transmitted back via the downlink channel. In addition, to save communication overhead, we deploy two a DRL-based two-stage point cloud data compressor on two UGVs, where the compression rate of two UGVs is dynamically and collaboratively determined based on the task requirements by another DRL agent deployed on the edge server.

#### B. Two-Stages Compression

As shown in Fig. 2, two UGVs capture the 3-D point cloud data of the front,  $\mathcal{X}^f(t) = \{x_1, x_2, \dots, x_m\}$ ,  $x_m \in \mathbb{R}^d$  and the rear,  $\mathcal{X}^r(t) = \{x_1, x_2, \dots, x_n\}$ ,  $x_n \in \mathbb{R}^d$  by the on-board lidar at a certain sensing rate in the  $t$ -th time slot, where  $d$  is the dimension. To compress the captured 3-D point cloud data to reduce the communication overhead, we introduce a two-stage DRL-based point cloud data compression module. Here we propose to use *PointNet++* as the static compressor for its simple structure, widespread application, and suitability for complex scene compression [29]. Specifically, firstly, in the  $t$ -th time slot,  $\mathcal{X}^f(t)$  and  $\mathcal{X}^r(t)$  passed through the feature extractor part of *PointNet++*, which is a hierarchical neural network expressed by

$$\bar{\mathcal{X}}^f(t) = f_{e1}(\mathcal{X}^f(t), \theta_{e1}), \quad (1)$$

$$\bar{\mathcal{X}}^r(t) = f_{e2}(\mathcal{X}^r(t), \theta_{e2}), \quad (2)$$

where  $\theta_{e1}, \theta_{e2}$  denote the parameters of the two feature extractors. Secondly,  $\bar{\mathcal{X}}^f(t)$  and  $\bar{\mathcal{X}}^r(t)$  are compressed to the vector  $\mathbf{x}^f(t)$  and  $\mathbf{x}^r(t)$  with a fixed latent space by passing

through two fully connected neural networks, separately, which is expressed by,

$$\mathbf{x}^f(t) = f_{s1}(\bar{\mathcal{X}}^f(t), \theta_{s1}), \quad (3)$$

$$\mathbf{x}^r(t) = f_{s2}(\bar{\mathcal{X}}^r(t), \theta_{s2}), \quad (4)$$

where  $f_{s1}(\cdot, \theta_{s1}), f_{s2}(\cdot, \theta_{s2})$  represent the dimensional reduction neural networks and  $\theta_{s1}, \theta_{s2}$  are the corresponding parameters.

For the second-stage model-based data compressor, we propose to use Latent Semantic Analysis (LSA) for its simplicity, robustness, and no need for extensive hyper-parameter tuning [30]. It works by decomposing a term-document matrix using Singular Value Decomposition (SVD) to reveal and map the underlying semantic structure into a lower-dimensional space. Specifically, in the  $t$ -th time slot,  $\mathbf{x}^f(t)$ , and  $\mathbf{x}^r(t)$  are firstly decomposed by SVD separately, which is denoted by

$$U_f(t)\Sigma_f(t)V_f^T(t) = \mathbf{x}^f(t), \quad (5)$$

$$U_r(t)\Sigma_r(t)V_r^T(t) = \mathbf{x}^r(t), \quad (6)$$

where  $U_f(t) \in \mathbb{R}^{1 \times 1}$  and  $U_r(t) \in \mathbb{R}^{1 \times 1}$  are the left singular vectors for the front and rear UGVs respectively,  $\Sigma_f(t) \in \mathbb{R}^{1 \times n}$  and  $\Sigma_r(t) \in \mathbb{R}^{1 \times n}$  are the diagonal matrices for the front and rear UGVs with non-negative singular values in descending order, and  $V_f^T(t) \in \mathbb{R}^{n \times n}$  and  $V_r^T(t) \in \mathbb{R}^{n \times n}$  are the right singular vectors for the front and rear UGVs, respectively. Secondly, by selecting the top  $k^f, k^r$  singular values from  $\Sigma_f(t), \Sigma_r(t)$ , and their corresponding vectors from  $U_f(t), U_r(t), V_f^T(t)$  and  $V_r^T(t)$ , we achieve the dimensionality reduction by operating the inverse of SVD,

$$\mathbf{z}_f(t) = U'_f(t)\Sigma'_f(t)V'^T_f(t), \quad (7)$$

$$\mathbf{z}_r(t) = U'_r(t)\Sigma'_r(t)V'^T_r(t), \quad (8)$$

where  $U'_f(t), U'_r(t) \in \mathbb{R}^{1 \times 1}$ ,  $\Sigma'_f(t) \in \mathbb{R}^{1 \times k^f(t)}$  and  $\Sigma'_r(t) \in \mathbb{R}^{1 \times k^r(t)}$  are the compressed diagonal matrices,  $V'^T_f(t) \in \mathbb{R}^{k^f(t) \times k^f(t)}$  and  $V'^T_r(t) \in \mathbb{R}^{k^r(t) \times k^r(t)}$  are the compressed right singular vectors, and  $k^f(t), k^r(t) \in \mathcal{Z}$  are the dynamic compression parameters. Thus, by synthesizing the information from results of (5), (6), (7), (8), the dynamic compression in the  $t$ -th time slot is expressed by

$$\{\mathbf{z}^f(t), \mathbf{z}^r(t)\} = f_d(\{\mathbf{x}^f(t), \mathbf{x}^r(t)\}, \theta_d, \{k^f(t), k^r(t)\}), \quad (9)$$

where  $f_d(\cdot, \theta_d)$  is the process of dynamic compressor,  $\theta_d$  represents the parameters of the compressor. To dynamically change the compression ratio, we deploy a DRL agent at the edge server to dynamically decide the value of  $k^f(t)$  and  $k^r(t)$  and send them back to each UGVs via wireless channel. The details will be provided in the following Section. After the two-stage compression, the compression ratio of  $\mathbf{z}^f(t)$  and  $\mathbf{z}^r(t)$  compared to original cloud point data  $\mathcal{X}^f(t)$  and  $\mathcal{X}^r(t)$  is given as

$$\rho^f(t) = \frac{k^f(t)}{m \cdot d}, \quad (10)$$

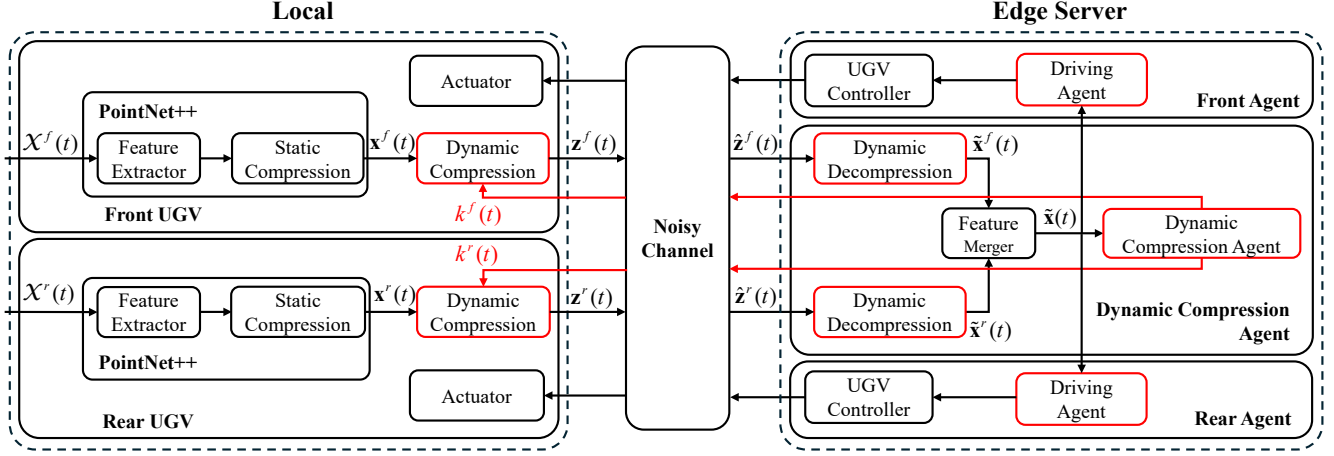


Fig. 2. Integrated Feature Extraction, Reinforcement Learning, and Data Compression in a Cooperative Semantic Communication System.

$$\rho^r(t) = \frac{k^r(t)}{n \cdot d}. \quad (11)$$

### C. Communication Model

The compressed data are transmitted to the edge server via wireless communications. Without loss of generality, we simplify the communication model by only considering the uplink latency and ignoring the latency for the downlink, since the communication resources spent on downlink including control commands and compress rate decision are often negligible. We also assume that the channel gain and transmission rate remain constant over a small time interval, and the two UGVs have i.i.d. channel conditions. Here, we take one of the UGV as an example, where the uplink transmission rate in the  $t$ -th time slot is given by

$$r_t(t) = B \cdot \log_2 \left( 1 + \frac{p(t) \cdot g(t)}{N_0} \right), \quad (12)$$

where  $B$  denotes the bandwidth allocated to the UGVs [31]. The signal-to-interference-plus-noise ratio (SINR) for the signals received at the edge server is expressed as

$$\text{SINR} = \frac{p(t) \cdot g(t)}{N_0}, \quad (13)$$

where  $p(t)$  is the transmission power of the UGVs, and  $N_0$  is the Additive White Gaussian Noise (AWGN). The channel gain for the signals received at the edge server is

$$g(t) = d^{-\alpha} u_t, \quad (14)$$

which accounts for the instantaneous perception of the communication environment. The distance  $d$  between the Jackal UGVs and the edge server is the most significant factor affecting the channel gain. The path loss exponent is denoted by  $\alpha$ , and  $u_t$  follows a Rayleigh distribution with a unit mean. The uplink transmission latency is then given by

$$T_{up} = \arg \min_{r(t)} \int_0^s r(t) dt \approx \frac{N^b}{r(t)}, \quad (15)$$

where  $N^b$  represents the total number of bits, the total number of bits  $N_f^b$  for front UGV and  $N_r^b$  for rear UGV are then given by

$$N_f^b = n^b \cdot k_f(t), \quad (16)$$

$$N_r^b = n^b \cdot k_r(t), \quad (17)$$

where  $n^b$  is the number of bits in each component,  $k_f(t)$  and  $k_r(t)$  are the number of components in the point cloud features after the second-stage compression  $\mathbf{z}^f(t)$  and  $\mathbf{z}^r(t)$ . Given that the transmission rate  $r_t(t)$  in each time slot under a stationary channel is constant, the latency can be approximated as the ratio of the number of transmitted bits  $N^b$  to  $r_t(t)$ .

### D. Edge Server

The edge server first receives the compressed point cloud feature  $\hat{\mathbf{z}}^f(t)$  and  $\hat{\mathbf{z}}^r(t)$  from the front UGV and rear UGV. With inversed LSA, the compressed point cloud features will be decompressed with

$$\begin{aligned} \tilde{\mathbf{x}}(t) &= [\tilde{\mathbf{x}}^f(t), \tilde{\mathbf{x}}^r(t)] \\ &= f_d^{-1}(\{\hat{\mathbf{z}}^f(t), \hat{\mathbf{z}}^r(t)\}, \theta_d, \{k^f(t), k^r(t)\}). \end{aligned} \quad (18)$$

In addition, we deploy three reinforcement learning agents on the edge server, which are responsible for the offload function 1) the front UGV for navigation 2) the rear UGV for collaborated conveyance, and 3) the compression ratio decision making, respectively. The two driving agents will infer driving commands for both UGVs with observation  $\tilde{\mathbf{x}}(t)$ , where for the front UGV the command is its angular speed  $\theta^f(t)$  and for the rear UGV is its angular and linear speeds  $\theta^r(t)$  and  $v^r(t)$ . Then  $\theta^f(t)$ ,  $\theta^r(t)$ , and  $v^r(t)$  will be sent to the two UGVs to be executed. More details about agent settings will be given in the next section.

## IV. PROBLEM FORMULATION

We propose a two-phase DRL algorithm for different task-oriented components. In the first phase, we train navigation

---

**Algorithm 1** Two-Phase DRL Training

---

1: **Input:** Initialize the navigation policy  $\pi_{\theta_1}$ , cooperative conveyance policy  $\pi_{\theta_2}$ , compression policy  $\pi_{\theta_3}$ , the parameters of neural network  $\theta_1, \theta_2$  and  $\theta_3$ , the positions of the UGVs and the cargo box  $\mathbf{p}_0^f, \mathbf{p}_0^r$  and  $\mathbf{p}_0^c$ , and the total training steps  $T_t$ .

2: **Phase 1:** Training policies  $\pi_{\theta_1}$  and  $\pi_{\theta_2}$ .

3: **for**  $t = 1, 2, \dots, T_t$  **do**

4:   Sample  $\mathcal{X}_f(t)$  and  $\mathcal{X}_r(t)$  from the front and rear UGVs.

5:    $\mathbf{x}_f(t) \leftarrow f_{s^1}(f_{e^1}(\mathcal{X}_f(t), \theta_{e^1}), \theta_{s^1})$ ,  
     $\mathbf{x}_r(t) \leftarrow f_{s^2}(f_{e^2}(\mathcal{X}_r(t), \theta_{e^2}), \theta_{s^2})$ .

6:    $\mathbf{x}(t) \leftarrow [\mathbf{x}_f(t), \mathbf{x}_r(t)]$ .

7:    $\mathbf{s}_t^{[1]} \leftarrow \mathbf{x}(t)$ ,  $\mathbf{s}_t^{[2]} \leftarrow \mathbf{x}(t)$ .

8:    $\mathbf{a}_t^{[1]} \leftarrow \pi_{\theta_1}(\mathbf{s}_t^{[1]})$ ,  $\mathbf{a}_t^{[2]} \leftarrow \pi_{\theta_2}(\mathbf{s}_t^{[2]})$ .

9:   Calculate  $r^{[1]}(\mathbf{s}_t^{[1]}, \mathbf{a}_t^{[1]})$  with (21),  
    and  $r^{[2]}(\mathbf{s}_t^{[2]}, \mathbf{a}_t^{[2]})$  with (25).

10:   Collect tuple  $\{\tilde{\mathbf{x}}_t, \mathbf{a}_t^{[1]}, \mathbf{a}_t^{[2]}, r^{[1]}(\mathbf{s}_t^{[1]}, \mathbf{a}_t^{[1]}), r^{[2]}(\mathbf{s}_t^{[2]}, \mathbf{a}_t^{[2]})\}$

11:   **if** Episode ends **then:**

12:     Calculate the Q-Values  $Q^{\pi_{\theta_1}}$  and  $Q^{\pi_{\theta_2}}$  with  
     $Q^{\pi_{\theta}}(\mathbf{s}_t, \mathbf{a}_t) \leftarrow \mathbb{E}[\sum_{t=0}^{\infty} \gamma^t r(\mathbf{s}_t, \mathbf{a}_t) \mid \pi_{\theta}]$ .

13:     Train  $\theta_1$  and  $\theta_2$  to maximize  $Q^{\pi_{\theta_1}}$  and  $Q^{\pi_{\theta_2}}$ .

14:   **end if**

15: **end for**

16: **Output:** Optimal policies  $\pi_{\theta_1}^*$  and  $\pi_{\theta_2}^*$ .

17: **Phase 2:** Training policy  $\pi_{\theta_3}$ .

18: **for**  $t = 1, 2, \dots, T_t$  **do**

19:   Sample and compress to get  $\mathbf{x}^f(t)$  and  $\mathbf{x}^r(t)$   
    with Step 4 to Step 5.

20:    $\{\mathbf{z}^f(t), \mathbf{z}^r(t)\} \leftarrow f_d(\{\mathbf{x}^f(t), \mathbf{x}^r(t)\}, \theta_d, \{k^f(t), k^r(t)\})$ .  
    Dynamic compression with (9).

21:   Calculate  $T_{up}$  with (15).

22:   Decompress  $\tilde{\mathbf{x}}(t)$  with (18).

23:    $\mathbf{s}_t^{[1]} \leftarrow \tilde{\mathbf{x}}(t)$ ,  $\mathbf{s}_t^{[2]} \leftarrow \tilde{\mathbf{x}}(t)$ ,  $\mathbf{s}_t^{[3]} \leftarrow [\tilde{\mathbf{x}}(t), g^f(t), g^r(t)]$

24:    $\mathbf{a}_t^{[1]} \leftarrow \pi_{\theta_1}^*(\mathbf{s}_t^{[1]})$ ,  $\mathbf{a}_t^{[2]} \leftarrow \pi_{\theta_2}^*(\mathbf{s}_t^{[2]})$ .

25:    $\mathbf{a}_t^{[3]} \leftarrow \pi_{\theta_3}(\mathbf{s}_t^{[3]})$ .

26:   Calculate  $r^{[3]}(\mathbf{s}_t^{[3]}, \mathbf{a}_t^{[3]})$  with (29).

27:   Collect tuple  $\{\tilde{\mathbf{x}}_t, g^f(t), g^r(t), \mathbf{a}_t^{[3]}, r^{[3]}(\mathbf{s}_t^{[3]}, \mathbf{a}_t^{[3]})\}$ .

28:   **if** Episode ends **then:**

29:     Calculate  $Q^{\pi_{\theta_3}}$  with  
     $Q^{\pi_{\theta}}(\mathbf{s}_t, \mathbf{a}_t) \leftarrow \mathbb{E}[\sum_{t=0}^{\infty} \gamma^t r(\mathbf{s}_t, \mathbf{a}_t) \mid \pi_{\theta}]$ .

30:     Train  $\theta_3$  to maximize  $Q^{\pi_{\theta_3}}$ .

31:   **end if**

32: **end for**

33: **Output:** Optimal policies for  $\pi_{\theta_3}^*$ .

---

agent  $\pi_{\theta_1}$  and for the navigation of the front UGV and collaborated conveyance agent  $\pi_{\theta_2}$  for the rear UGV, respectively. In the second phase, we train the dynamic compression agent  $\pi_{\theta_3}$  with optimal  $\pi_{\theta_1}^*$  and  $\pi_{\theta_2}^*$ .  $\pi_{\theta_3}$  determines the optimal task-oriented compression ratio for the dynamic compression algorithm.

### A. Navigation

The navigation agent with DRL policy  $\pi_{\theta_1}$  navigates the front path and produces  $\theta^f(t)$  and ensures that it reaches the given target position.

1) *State:* In the  $t$ -th time slot, the state of  $\pi_{\theta_1}$  agent is

$$\mathbf{s}_t^{[1]} = \tilde{\mathbf{x}}(t), \quad (19)$$

where  $\tilde{\mathbf{x}}(t) \in [0, 1]^{1 \times n}$  is the normalized decompressed point cloud data at the edge server with  $1 \times n$  dimensions.

2) *Action:* The action in the  $t$ -th time slot of  $\pi_{\theta_1}$  agent is the normalized angular velocity of the front UGV

$$\mathbf{a}_t^{[1]} = \theta^f(t), \quad (20)$$

where  $\theta^f(t) \in [0, 1]$  is the angular speed command for the front UGV.

3) *Reward:* The reward of  $\pi_{\theta_1}$  agent is given by

$$r^{[1]}(\mathbf{s}_t^{[1]}, \mathbf{a}_t^{[1]}) = w_1 \cdot \text{MSE}(\mathbf{p}^f(t), \mathbf{p}_{tar}^f) + w_2 \cdot |\phi^f(t) - \phi_{tar}^f|, \quad (21)$$

where  $\mathbf{p}^f(t) = [x^f(t), y^f(t)]$  is the position of the front UGV in the  $t$ -th timeslot,  $\mathbf{p}_{tar}^f = [x_{tar}^f, y_{tar}^f]$  is its target position;  $\phi^f(t)$  and  $\phi_{tar}^f$  are the orientation of the front UGV in the  $t$ -th timeslot and the target orientation. The  $\text{MSE}(\cdot, \cdot)$  operator denotes the Mean Squared Error (MSE) of two positions, defined as

$$\text{MSE}(\mathbf{p}_1, \mathbf{p}_2) = \sqrt{(x_1 - x_2)^2 + (y_1 - y_2)^2}. \quad (22)$$

### B. Cooperative Conveyance

The cooperative conveyance agent with DRL policy  $\pi_{\theta_2}$  controls the rear UGV and ensures that it follows the front UGV and gives adequate force to the parcel so that it is held between the two Jackals in the same trajectory.

1) *State:* In the  $t$ -th time slot, the state of  $\pi_{\theta_2}$  agent is

$$\mathbf{s}_t^{[2]} = \tilde{\mathbf{x}}(t). \quad (23)$$

2) *Action:* The action in the  $t$ -th time slot of  $\pi_{\theta_2}$  agent is the normalized angular and linear velocity of the rear UGV

$$\mathbf{a}_t^{[2]} = [\theta^r(t), v^r(t)], \quad (24)$$

where  $\theta^r(t) \in [0, 1]$  and  $v^r(t) \in [0, 1]$  are the normalized angular and linear velocities for the rear UGV, respectively.

3) *Reward:* The reward of  $\pi_{\theta_2}$  agent is given by

$$r^{[2]}(\mathbf{s}_t^{[2]}, \mathbf{a}_t^{[2]}) = w_3 \cdot \text{MSE}(\mathbf{p}^f(t), \mathbf{p}^r(t)) + w_4 \cdot \text{MSE}(\mathbf{p}^c(t), \mathbf{p}^r(t)) + w_5 \cdot p_m, \quad (25)$$

where  $\mathbf{p}^r(t) = [x^r(t), y^r(t)]$  is the position of the rear UGV in the  $t$ -th timeslot,  $\mathbf{p}^c(t) = [x^p(t), y^p(t)]$  is the position of the cargo box in the  $t$ -th timeslot, and  $p_m$  is a penalty given when the orientations of the two UGVs are misaligned over a threshold  $\phi_T$ , denoted as

$$p_m = \begin{cases} 0, & \text{when } |\phi^f(t) - \phi^r(t)| < \phi_T, \\ -1, & \text{otherwise.} \end{cases} \quad (26)$$

### C. Dynamic Compression

In the  $t$ -th time slot, the compression ratio  $\rho^f$  and  $\rho^r$  is decided by the dynamic compression agent with DRL policy  $\pi_{\theta_3}$ .

1) *State*: In the  $t$ -th time slot, the state of  $\pi_{\theta_3}$  agent is the merged decompressed point cloud data with the channel gains:

$$\mathbf{s}_t^{[3]} = [\tilde{\mathbf{x}}(t), g^f(t), g^r(t)], \quad (27)$$

where  $\tilde{\mathbf{x}}(t) \in [0, 1]^{1 \times n}$  is the merged decompressed point cloud data with  $1 \times n$  dimensions,  $g^f(t)$  and  $g^r(t)$  are the channel gains of front and rear UGVs, respectively.

2) *Action*: The action in the  $t$ -th time slot of  $\pi_{\theta_3}$  agent is the compression parameters for both dynamic compressors, denoted by

$$\mathbf{a}_t^{[3]} = [k^f(t), k^r(t)], \quad (28)$$

where  $k^f(t)$  and  $k^r(t)$  are the compression parameters for the front and rear UGVs, respectively.

3) *Reward*: The reward of  $\pi_{\theta_3}$  agent is a weighted sum of the distance between the cargo box and the loading area and the communication cost, denoted by

$$r_t^{[3]}(\mathbf{s}_t^{[3]}, \mathbf{a}_t^{[3]}) = w_6 \cdot \text{MSE}(\mathbf{p}^c(t), \mathbf{p}_{tar}^c) - w_7 \cdot \max(T_{up}^f, T_{up}^r), \quad (29)$$

where  $\mathbf{p}_{tar}^c$  is the target position of the cargo box and  $T_{up}$  is the uplink transmission latency in the  $t$ -th time slot.

### D. Solution

The proposed two-phase DRL problem is shown in Algorithm 1 based on the Proximal Policy Optimization (PPO) algorithm [32]. We pre-train two *PointNet++* neural networks by embedding individual DRL in the experiment environment without the integration of three agents.

In the phase 1, after the feature vector  $\tilde{\mathbf{x}}_t$  is transmitted to the edge server, the  $\pi_{\theta_1}$  and  $\pi_{\theta_2}$  generate  $\mathbf{a}_t^{[1]}$  with the observation  $\tilde{\mathbf{x}}_t$  simultaneously, and  $\mathbf{a}_t^{[2]}$  transmit them back to UGVs. Then, by executing  $\mathbf{a}_t^{[1]}$  and  $\mathbf{a}_t^{[2]}$ , the instantaneous rewards  $r_t^{[1]}(\mathbf{s}_t^{[1]}, \mathbf{a}_t^{[1]})$  and  $r_t^{[2]}(\mathbf{s}_t^{[2]}, \mathbf{a}_t^{[2]})$  are also obtained. Thus, by sampling the batch from the collected tuple  $\{\tilde{\mathbf{x}}_t, \mathbf{a}_t^{[1]}, \mathbf{a}_t^{[2]}, r_t^{[1]}(\mathbf{s}_t^{[1]}, \mathbf{a}_t^{[1]}), r_t^{[2]}(\mathbf{s}_t^{[2]}, \mathbf{a}_t^{[2]})\}$  and train  $\theta_1$  and  $\theta_2$ ,  $\pi_{\theta_1}^*$  and  $\pi_{\theta_2}^*$  are obtained. In the phase 2, with the optimal and fixed  $\pi_{\theta_1}^*$  and  $\pi_{\theta_2}^*$  obtained in the phase 1,  $\pi_{\theta_3}$  is optimized by sampling the batch from the collected tuple  $\{\tilde{\mathbf{x}}_t, g^f(t), g^r(t), \mathbf{a}_t^{[3]}, r_t^{[3]}(\mathbf{s}_t^{[3]}, \mathbf{a}_t^{[3]})\}$ .

## V. EXPERIMENTAL SETUP

To evaluate the performance of the proposed framework, we establish our simulation platform on Nvidia Isaac Sim [33] for its realistic physical simulator and integral interface for robotic systems. As shown in Fig. 3, two Clearpath Jackal UGVs [34] are modeled in a warehouse environment. Notably, for each Jackal, a plate is mounted on the front/rear side with a hinge to allow passive rotations at  $\pm 30$  degs. The plates help the Jackal UGVs curve without releasing the carried cargo box. The two Jackal UGVs with their attached plates

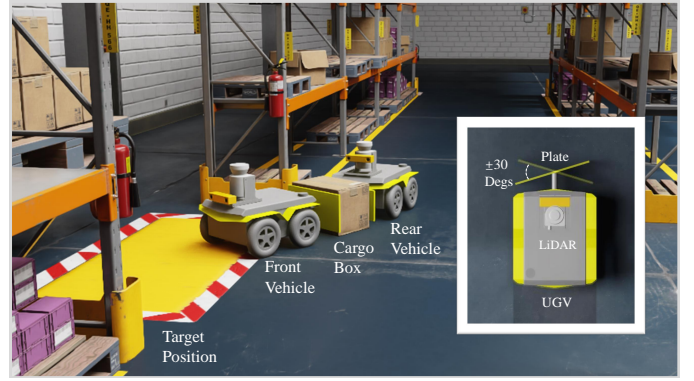


Fig. 3. Prototype design in Isaac Sim (The demonstration video is available at <https://youtu.be/egElaBiVmpA>).

together make our cooperative conveyance system [13] for cargo boxes in the proposed framework. The sensory system is built by two LiDARs mounted on the top of each Jackal UGV. Point cloud data will be sampled by each LiDAR at a certain frequency. The task in this experiment is to move the cargo box with our conveyance system to the target position, which is labeled as the yellow zone in Fig. 3. In each time slot, the channel gains  $g^f(t)$  and  $g^r(t)$  are sampled from an average distribution, with values taken from  $\{-30\text{dB}, -20\text{dB}, -10\text{dB}, 0\text{dB}, 10\text{dB}, 20\text{dB}, 30\text{dB}\}$ . The dynamic channel compression parameter  $k^f(t)$  and  $k^r(t)$  takes value from  $\{1, 2, 3, \dots, 127\}$ . Thus, the compressed normalized point cloud feature has  $k^f(t)$  and  $k^r(t)$  components in float32 where each float32 data type consists of 32 bits.

## VI. SIMULATION RESULT

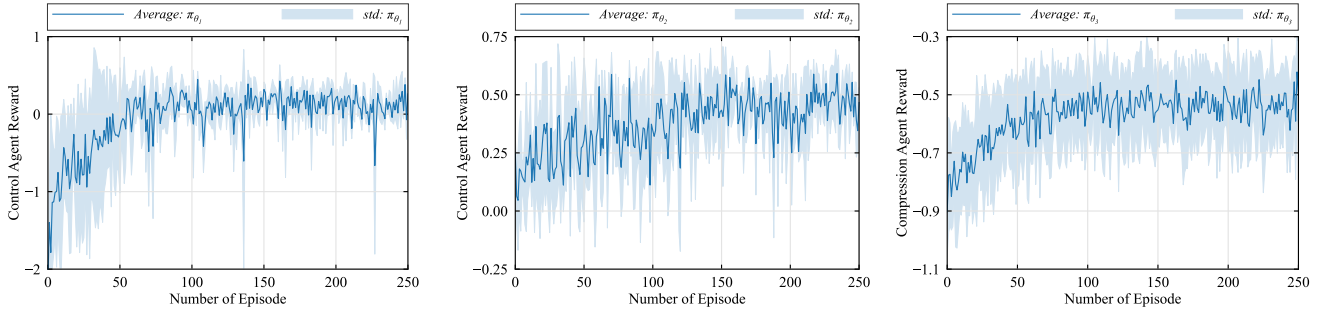
We evaluate 1) the performance of DRL training process for  $\pi_{\theta_1}$ ,  $\pi_{\theta_2}$  and  $\pi_{\theta_3}$ . 2) the task completion rate for the cooperative conveyance system with the integration of  $\pi_{\theta_3}$ . 3) the effectiveness of the proposed  $\pi_{\theta_3}$ .

### A. Evaluation of Task Completion

As shown in Fig. 4(a) and Fig. 4(b), to evaluate the performance of task completion for two Jackals UGVs without the compression DRL module, we simultaneously train the dual PPO algorithms for two Jackals UGVs control agents,  $\pi_{\theta_1}$  and  $\pi_{\theta_2}$ , over 250 episodes for 3 times.  $\pi_{\theta_1}$  converged after 80 training epochs, while  $\pi_{\theta_2}$  converged after 140 training epochs.

### B. Evaluation of Compression Agent

Fig. 4(c) illustrates the changes in the average reward and its standard deviation for  $\pi_{\theta_3}$ . The average reward value generally shows an upward trend, and the fluctuations of the compression ratio gradually decrease. Additionally, Fig. 6 displays the changes in the compression parameters over 250 training episodes. Both compression ratios  $\rho^f$  and  $\rho^r$  decrease during the training process and converge at  $k^f = 19$ ,  $k^r = 22$  after 185 training episodes, which means that the overall



(a) Average reward per step in each training episode for front control agent  $\pi_{\theta_1}$ . (b) Average reward per step in each training episode for rear control agent  $\pi_{\theta_2}$ . (c) Average reward per step in each training episode for compression agent  $\pi_{\theta_3}$ .

Fig. 4. Performance evaluation for three DRL agent  $\pi_{\theta_1}$ ,  $\pi_{\theta_2}$  and  $\pi_{\theta_3}$ .

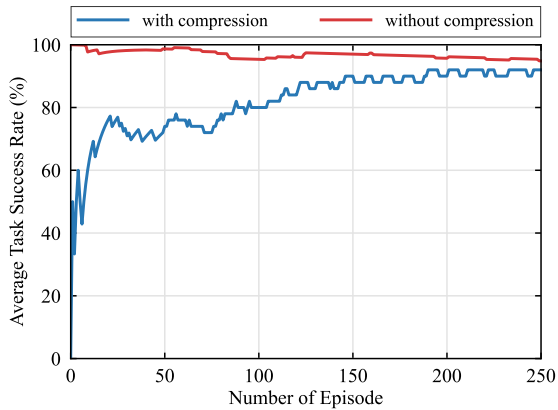


Fig. 5. Average task success rate in each training episode.

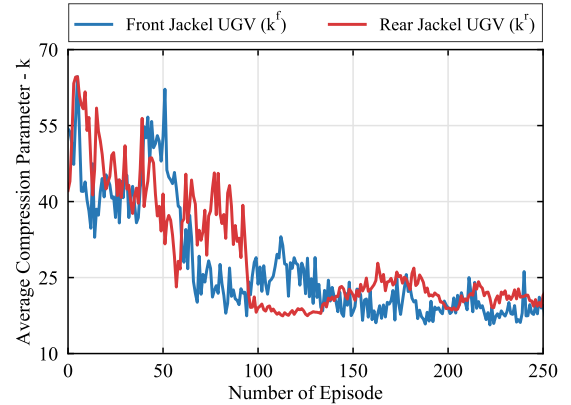


Fig. 6. Average compression Parameter in each training episode.

compression ratio decreases to approximately 0.32% compared to the raw point cloud data, which initially consisted of approximately 20,000 points before compression.

### C. Evaluation of Task completion performance under Dynamic Compression

As shown in Fig. 5, we evaluate the task completion rate after incorporating the compression agent. Specifically, we define the average task success rate as the number of successful attempts out of 100 repetitions of the experiment in the current training episode. The weights for  $\pi_{\theta_3}$ , are set to  $\omega_6 = 0.8$  and  $\omega_7 = 0.2$ . The reward of both two control agents for two Jackals UGVs converges after training of 130 episodes. Our proposed framework successfully completes the task with an approximate average task success rate of 90% after convergence, which is close to the success rate without the compression model.

### D. Evaluation of Different Weights

We further evaluate the robustness of the proposed framework by adjusting different weights  $\omega_6$  and  $\omega_7$ . Tab. ?? shows the results with varying weights  $\omega_6$  and  $\omega_7$ . As  $\omega_6$  increases from  $\omega_6 = 0.5$  to 0.99 and  $\omega_7$  decreases from  $\omega_7 = 0.5$

TABLE I  
EVALUATION OF DIFFERENT WEIGHT

$\omega_6$	0.99	0.9	0.8	0.7	0.6	0.5
$\omega_7$	0.01	0.1	0.2	0.3	0.4	0.5
success rate (%)	96	93	91	82	69	53
average $k^f(t)$	103	43	19	14	7	6
average $k^r(t)$	110	49	22	11	9	5

to 0.01, the task success rate increases significantly to 96%. However, the average compression parameter  $k^f(t)$  and  $k^r(t)$  will increase with, occupying more communication load.

## VII. CONCLUSION

We presented a task-oriented edge-assisted cooperative data compression, communication, and computing framework for UGV-enhanced warehouse logistics. The warehouse logistics collaboration task, where two UGVs cooperatively carry a cargo box to the target position, was successfully offloaded to the edge server. In addition, a two-stage DRL-based point cloud data compression algorithm was deployed on the edge server and the UGVs, where the dynamic compression ratio of two UGVs  $\rho^f$  and  $\rho^r$  was dynamically and collaboratively determined based on the task requirements. The experimental

result showed that the system can complete the task with a success rate of 90% with the compression module ( $\omega_6 = 0.8$ ,  $\omega_7 = 0.2$ ), with an average compression ratio of 3.2% after the static compression and an average compression ratio of 0.3% after the dynamic compression.

#### REFERENCES

- [1] G. Richards, *Warehouse Management: A Complete Guide to Improving Efficiency and Minimizing Costs in the Modern Warehouse*. 2017.
- [2] NVIDIA, "Ai-enabled warehouse logistics," NVIDIA, 2024, <https://www.nvidia.com/en-gb/industries/retail/warehouse-logistics/>.
- [3] "Study on scenarios and requirements for next generation access technologies," document 3GPP, TSG RAN TR38.913 R14, 2017.
- [4] D. C. Nguyen, M. Ding, P. N. Pathirana, *et al.*, "6g internet of things: A comprehensive survey," *IEEE Internet Things J.*, vol. 9, no. 1, pp. 359–383, 2022.
- [5] Y. Mao, C. You, J. Zhang, K. Huang, and K. B. Letaief, "A survey on mobile edge computing: The comm. perspective," *IEEE Commun. Surv. Tutor.*, vol. 19, no. 4, pp. 2322–2358, 2017.
- [6] H. T. Dinh, C. Lee, D. Niyato, and P. Wang, "A survey of mobile cloud computing: Architecture, applications, and approaches," *Wirel. Commun. Mob. Comput.*, vol. 13, no. 18, pp. 1587–1611, 2013.
- [7] X. Chen, H. Zhang, C. Wu, S. Mao, Y. Ji, and M. Bennis, "Optimized computation offloading performance in virtual edge computing systems via deep reinforcement learning," *IEEE Internet Things J.*, vol. 6, no. 3, pp. 4005–4018, 2019.
- [8] C. Chaccour, W. Saad, M. Debbah, Z. Han, and H. V. Poor, "Less data, more knowledge: Building next generation semantic comm. networks," *IEEE Commun. Surv. Tutor.*, pp. 1–1, 2024.
- [9] D. Gündüz, Z. Qin, I. E. Aguerri, *et al.*, "Beyond transmitting bits: Context, semantics, and task-oriented comm.," *IEEE J. Sel. Areas Commun.*, vol. 41, no. 1, pp. 5–41, 2023.
- [10] Z. Meng, K. Chen, Y. Diao, *et al.*, "Task-oriented cross-system design for timely and accurate modeling in the metaverse," *IEEE J. Sel. Areas Commun.*, vol. 42, no. 3, pp. 752–766, 2024.
- [11] Y. Diao, Z. Meng, X. Xu, C. She, and P. G. Zhao, "Task-oriented source-channel coding enabled autonomous driving based on edge computing," *IEEE INFOCOM 2024-IEEE Conf. Comput. Commun. Workshops (INFOCOM WKSHPs)*, 2024.
- [12] Z. Meng, C. She, G. Zhao, *et al.*, "Task-oriented metaverse design in the 6g era," *IEEE Wirel. Commun.*, vol. 31, no. 3, pp. 212–218, 2024.
- [13] T. Kumagai, S. Yasuda, and H. Yoshida, "A prototype of a cooperative conveyance system by wireless-network control of multiple robots," in *IECON 2019 - 45th Annual Conf. IEEE Ind. Electron. Soc.*, vol. 1, 2019, pp. 231–236.
- [14] L. He, G. Sun, Z. Sun, *et al.*, *Qoe maximization for multiple-uav-assisted multi-access edge computing: An online joint optimization approach*, 2024. arXiv: 2406.11918.
- [15] Y. Qiao, Y. Fu, and M. Yuan, "Comm.-control co-design in wireless networks: A cloud control agv example," *IEEE Internet Things J.*, vol. 10, no. 3, pp. 2346–2359, 2023.
- [16] S. Liu, Y. Yu, X. Lian, *et al.*, "Dependent task scheduling and offloading for minimizing deadline violation ratio in mobile edge computing networks," *IEEE J. Sel. Areas Commun.*, vol. 41, no. 2, pp. 538–554, 2023.
- [17] M. Penmetcha and B.-C. Min, "A deep reinforcement learning-based dynamic computational offloading method for cloud robotics," *IEEE Access*, vol. 9, pp. 60 265–60 279, 2021.
- [18] H. Xie, Z. Qin, X. Tao, G. Lu, and D. Wu, "Deepsc: Deep learning enabled semantic comm. systems," *IEEE Trans. Wireless Commun.*, vol. 20, no. 8, pp. 5120–5133, 2021.
- [19] W. Zhang, Y. Wang, M. Chen, T. Luo, and D. Niyato, "Optimization of image transmission in cooperative semantic comm. networks," *IEEE Trans. Wireless Commun.*, vol. 23, no. 2, pp. 861–872, 2024.
- [20] J. Shao, H. Zhang, Y. Mao, and J. Zhang, "Branchy-gnn: A device-edge co-inference framework for efficient point cloud processing," in *ICASSP 2021 - 2021 IEEE Int. Conf. Acoust., Speech Signal Process. (ICASSP)*, 2021, pp. 8488–8492.
- [21] Y. Xu, H. Zhou, and Y. Deng, "Task-oriented semantics-aware communication for wireless uav control and command transmission," *IEEE Commun. Lett.*, vol. 27, no. 8, pp. 2232–2236, 2023.
- [22] P. Talli, F. Pase, F. Chiariotti, A. Zanella, and M. Zorzi, "Effective comm. with dynamic feature compression," *IEEE Trans. Commun.*, pp. 1–1, 2024.
- [23] J. Shao, Y. Mao, and J. Zhang, "Learning task-oriented communication for edge inference: An information bottleneck approach," *IEEE J. Sel. Areas Commun.*, vol. 40, no. 1, pp. 197–211, 2022.
- [24] A. Mostaani, T. X. Vu, H. Habibi, S. Chatzinotas, and B. Ottersten, "Task-oriented communication design at scale," *IEEE Trans. Commun.*, pp. 1–1, 2024.
- [25] G. He, M. Feng, Y. Zhang, G. Liu, Y. Dai, and T. Jiang, "Deep reinforcement learning based task-oriented communication in multi-agent systems," *IEEE Wirel. Commun.*, vol. 30, no. 3, pp. 112–119, 2023.
- [26] Y. E. Sagduyu, T. Erpek, A. Yener, and S. Ulukus, "Multi-receiver task-oriented communications via multi-task deep learning," in *2023 IEEE Future Netw. World Forum (FNWF)*, 2023, pp. 1–6.
- [27] J. Shao, Y. Mao, and J. Zhang, "Task-oriented communication for multidevice cooperative edge inference," *IEEE Trans. Wirel. Commun.*, vol. 22, no. 1, pp. 73–87, 2023.
- [28] H. Xie, Z. Qin, X. Tao, and K. B. Letaief, "Task-oriented multi-user semantic communications," *IEEE J. Sel. Areas Commun.*, vol. 40, no. 9, pp. 2584–2597, 2022.
- [29] C. R. Qi, L. Yi, H. Su, and L. J. Guibas, "Pointnet++: Deep hierarchical feature learning on point sets in a metric space," in *Adv. Neural Inf. Process. Syst.*, vol. 30, 2017.
- [30] P. W. F. Thomas K Landauer and D. Laham, "An introduction to latent semantic analysis," *Discourse Processes*, vol. 25, no. 2–3, pp. 259–284, 1998.
- [31] C. E. Shannon, "A mathematical theory of communication," *Bell Syst. Tech. J.*, vol. 27, no. 3, pp. 379–423, 1948.
- [32] J. Schulman, F. Wolski, P. Dhariwal, A. Radford, and O. Klimov, "Proximal policy optimization algorithms," *arXiv preprint arXiv:1707.06347*, 2017.
- [33] *What is Isaac Sim?* <https://docs.omniverse.nvidia.com/isaac-sim/latest/index.html>, (accessed Feb. 2024).
- [34] *Jackal: Unmanned Ground Vehicle*, <https://clearpathrobotics.com/jackal-small-unmanned-ground-vehicle/>, (accessed Jul. 2024).